Birefringence images of screw dislocations viewed end-on in cubic crystals

doi: 10.1063/1.347573

Birefringence images of screw dislocations viewed end-on in cubic crystals

Chuan-zhen Ge
National Laboratory of Solid State Microstructures and Department of Physics, Nanjing University, Nanjing 210008, People's Republic of China

Nai-ben Ming
National Laboratory of Solid State Microstructures and Department of Physics, Nanjing University, Nanjing 210008, People's Republic of China, and Center for Condensed Matter Physics and Radiation Physics, China Center of Advanced Science and Technology (World Laboratory), P.O. Box 8730, Beijing, People's Republic of China

K. Tsukamoto, K. Maiwa, and I. Sunagawa
Institute of Mineralogy, Petrology and Economic Geology, Tohoku University, Sendai 980, Japan

(Received 3 January 1991; accepted for publication 11 February 1991)

The expressions for the intensity distribution in birefringence images and computer-simulated images of a straight, pure screw dislocation with Burgers vector $a[111]$ viewed end-on in cubic crystals have been obtained for the first time by considering the anisotropy of both elastic and photoelastic properties of the material. The effect of elastic and photoelastic anisotropy on birefringence images of screw dislocation viewed end-on has been discussed. And the computer-simulated images have been compared with the experimental images observed in $Ba(NO_3)_2$ crystals grown from aqueous solution.

I. INTRODUCTION

Since birefringence topography was first used to image the stress fields of individual edge dislocations viewed end-on by Bond and Andrus,[1] much theoretical and experimental work has been done. Bullough[2] calculated the image contrast for such defects. Indenbom, Nikitenko, and Mitevskii[3] showed that the slip plane and the sense of the Burgers vector could be identified by their contrast behavior. Fathers and Tanner developed a theory of stress-birefringence image due to both screw and edge dislocations viewed from the side for anisotropic crystals[4] and isotropic crystals[5] which were verified with their own experiments[5] and other's observations.[6,7] Stacking faults,[8] inclusions,[5,9,10] magnetic domain walls,[11] ferroelectric domain walls,[4] twin lamellae, and grain boundaries[11] were also characterized by birefringence topography. With the development of magneto-optic devices, solid state laser devices and electro-optic semiconductor devices, this technique has become an important method for the characterization of defects in the crystals related to these devices, such as garnet crystals[5,6,9–24] and III-V compounds.[25–33] However, birefringence topography has rarely been employed for *in situ* observation of crystal growth or dissolution except in a few cases.[34] This is because all previous theoretical treatments of stress birefringence contrast due to dislocations have predicted that screw dislocations viewed end-on, which play an important role in crystal growth or dissolution, will be invisible. Recently, Ge and co-workers demonstrated both experimental and theoretically that birefringence images of a screw dislocation viewed end-on are visible in an elastically isotropic but photo-elastically anisotropic material[12] that contains a long-range plane stress field.[13] In this article an account will be given of results obtained theoretically for the birefringence image of a screw dislocation with Burgers vector $a[111]$ viewed end-on in cubic crystals by considering the anisotropy of both elastic and photoelastic properties of this material, which have been compared with experimental image observed in $Ba(NO_3)_2$ crystals grown from aqueous solution.

II. STRESS BIREFRINGENCE

In any given coordinate system, the equation of the index ellipsoid in the unstressed perfect crystal, including cubic, tetragonal, hexagonal, and trigonal crystal is

$$B_1^0X^2 + B_2^0Y^2 + B_3^0Z^2 + 2B_4YZ + 2B_5^0ZX + 2B_6^0XY = 1,$$

where B_m^0 $(m=1,2,...,6)$ are the elements of the relative dielectric impermeability tensor that are equal to the inverse of the dielectric tensor ϵ_m $(1,2,...,6)$. In the principal coordinate system, the off-diagonal elements vanish, and we have

$$B_m^0 = \epsilon_m^{-1} = n_m^{-2} \quad (m=1,2,3),$$

where n_m $(m=1,2,3)$ are principal refractive indices of the crystal. For an unstressed perfect cubic crystal, $n_1=n_2=n_3=n_0$, which means that such a crystal is an optically isotropic medium and its index ellipsoid is a sphere.

It is assumed that the propagation law of electric-magnetic wave in an anisotropic homogeneous medium can be applied to a crystal subjected to a stress of a dislocation and the stress field only changes the shape, size, and orientation of the index ellipsoid by the photoelastic effect, On applying the stress field of a dislocation, the ellipsoid is changed into another one whose equation may be written as

$$B_1X^2 + B_2Y^2 + B_3Z^2 + 2B_4YZ + 2B_5ZX + 2B_6XY = 1.$$

 0021-8979/91/117556-09$03.00

The small change of refractive index may be produced by the stress field of a dislocation. This change is mostly conveniently specified by giving the small changes on the coefficients B_m ($m=1,2,...,6$). And we have

$$B_m=B_m^0+\Delta B_m \quad (m=1,2,3,...6). \tag{1}$$

If we neglect higher-order terms than the first in the stress field of dislocations, the small changes on the coefficients can be written as

$$\Delta B_m=\Pi_{mn}\sigma_n \quad (m,n=1,2,3,...6), \tag{2}$$

where Π_{mn} are the piezooptical coefficients and σ_n are the stresses around a dislocation. It is worth noting that we have to transform the component of the piezo-optical tensor, Π_{mn}, and the stress tensor of a dislocation, σ_n, to the given coordinate system.

In order to determine the three principle axes, we take the defining property of principle axes that, at their intersections with the ellipsoid, the normal to the ellipsoid is parallel to the radius vector. The condition can be written as[35]

$$\begin{vmatrix} B_1-1/n^2 & B_6 & B_5 \\ B_6 & B_2-1/n^2 & B_4 \\ B_5 & B_4 & B_3-1/n^2 \end{vmatrix}=0. \tag{3}$$

This cubic equation in $(1/n^2)$ is called the secular equation. The three roots, n_1, n_2, n_3, say, define three directions in which the radius vector of the ellipsoid is parallel to the normal, that is, three principal axes. For light propagating in the Z direction of the given coordinate system, the secular equation becomes

$$\begin{vmatrix} B_1-1/n^2 & B_6 \\ B_6 & B_2-1/n^2 \end{vmatrix}=0. \tag{4}$$

This yields the major axis and minor axis of the intersection ellipse of the plane normal to the direction of light propagation, the Z axis, with the index ellipsoid. The two allowed polarization directions are parallel to the axes of the ellipse and consequently perpendicular to the direction of light propagation as well as to each other. The two waves polarized along these direction have, respectively, refractive indices, n_1 and n_2, which can be determined by two roots, $1/n_1^2$ and $1/n_2^2$, of Eq. (4). Thus the difference between n_1 and n_2 and an angle α between the x axis in a given coordinate system and the major axis of the ellipse is given approximately by

$$n_2-n_1=(n_0^3/2)[(B_2-B_1)^2+4B_6^2]^{1/2},$$

$$2\alpha=\tan^{-1}[2B_6/(B_2-B_1)]. \tag{5}$$

The intensity distribution in the birefringence image under crossed polars[36] is

$$I=a^2\sin^2(2\phi)\sin^2(\delta/2), \tag{6}$$

where a is the amplitude of the incident plane-polarized light, ϕ is the angle between vibration direction of the polarizer and semimajor axis of the ellipse, δ is the phase

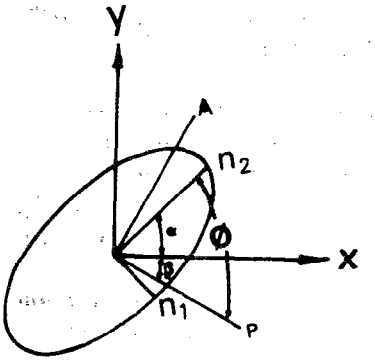

FIG. 1. Construction for finding indices of refraction and two allowed polarizations for the given direction of light propagation, Z axis. The ellipse is the intersection of the X-Y plane with the index ellipsoid.

difference between the two waves emerging from the wafer with thickness Δl, which can be written as

$$\delta=(2\pi/\lambda)(n_2-n_1)\Delta l$$

$$=(\pi n_0^3\Delta l/\lambda)[(B_2-B_1)^2+4B_6^2]^{1/2}, \tag{7}$$

where λ is the wavelength of the incident light. In general, δ is small and thus $\sin(\delta/2)=\delta/2$. If β is the angle between the vibration direction of the polarizer and X axis, $\phi=\alpha+\beta$, as shown in Fig. 1. In this case, Eq. (6) can be expressed as

$$I=[(\pi^2a^2n_0^6\Delta l^2)/(4\lambda^2)][(B_2-B_1)^2+4B_6^2]$$

$$\times\sin^2(2\beta+2\alpha),$$

$$2\alpha=\tan^{-1}[2B_6/(B_2-B_1)]. \tag{8}$$

Equation (8) is an expression for the intensity distribution in birefringence images of any type of dislocations in a crystal (not only cubic crystal). In principle, the stress field, σ_m, for a given type of dislocation in a given crystal can be known, thus, the ΔB_m, B_m, then the distribution of intensity in birefringence images, I, can be obtained according to Eqs. (2), (1), and (8).

III. BIREFRINGENCE IMAGES OF A ⟨111⟩ SCREW DISLOCATION IN CUBIC CRYSTALS

In general for elastically anisotropic cubic materials, such as $Ba(NO_3)_2$ crystal, only three independent constants are required, that is, the elastic compliance constants: s_{11},s_{12},s_{44}, or elastic stiffness constant: c_{11},c_{12},c_{44} in a physical coordinate system x,y,z along [100], [010], and [001]. In this article, we shall take these as one absolute magnitude (say c_{44}) and two ratios. One of these ratios is related to Poisson's ratio, $N=-s_{12}/s_{11}=c_{12}/(c_{11}+c_{12})$. The other more truly represents the elastically anisotropy and is $A=2(s_{11}-s_{12})/s_{44}=2c_{44}/(c_{11}-c_{12})$, which is also known as the Zener ratio.

The intensity distribution in the birefringence image of a straight dislocation in anisotropic media is most easily analyzed if the Z axis of a coordinate system is oriented parallel to the dislocation line and the direction of light propagation as well (viewed end-on), which may be called a dislocation coordinate system. For a straight screw dislocation with Burgers vector a[111], it is most convenient to use a dislocation coordinate system, X, Y, Z, with Z

parallel to the direction of the dislocation line and light propagation, [111], and X,Y along $[11\bar{2}]$ and $[\bar{1}10]$, respectively. First of all, our task is to find out how the values of components of two fourth rank tensors, the elastic stiffness constant c_{mn} and the piezo-optical coefficient Π_{mn} $(m,n=1,2,3,...6)$, transform when the coordinate system is transformed from [100], [010], [001], to $[11\bar{2}]$, $[\bar{1}10]$, [111]. The transformation of c_{mn} and Π_{mn} is shown in the Appendix.

The stress field of a straight, pure screw dislocation with a $\langle 111\rangle$ Burgers vector in an elastically anisotropic cubic crystal with infinite size and without any external loads has been obtained by Chou and Mitchell.[37] On choosing the dislocation coordinate system and following Chou,[37] the stress components of a screw dislocation, σ_m $(m=1,2,3,...,6)$, can be written as

$$\sigma_1=(bR^2S_{15}/2\pi S_{11}S_{44})[x^2y(3x^2-y^2)/Q],$$

$$\sigma_2=(bR^3S_{15}/2\pi S_{11}S_{44})[y^3(3x^2-y^2)/Q],$$

$$\sigma_3=-(bR^3S_{15}/2\pi S_{11}S_{44})[(s_{12}+\eta/3)/(s_{11}-2\eta/3)]\times[y(x^2+y^2)(3x^2-y^2)/Q],$$

$$\sigma_4=(bR/2\pi S_{44})(x/Q)[(x^2-y^2)(x^2-3y^2)+2R^2y^2(3x^2-y^2)],$$

$$\sigma_5=(bR/2\pi S_{44})(y/Q)\times[2x^2(x^2-3y^2)-R^2(x^2-y^2)(3x^2-y^2)],$$

$$\sigma_6=(bR^3S_{15}/2\pi S_{11}S_{44})[xy^2(3x^2-y^2)/Q], \tag{9}$$

where $Q=x^2(x^2-3y^2)^2+R^2y^2(3x^2-y^2)^2$ and $S_{mn}(m,n=1,2,3,...,6)$ are the modified elastic complications, which are convenient for the plane strain problem, are defined by Stroh.[38] When one principal strain is zero a crystal is said to be in a state of plane strain. Pure shear is a special case of plane strain, and a pure screw dislocation is just so. S_{mn} are related to the three independent elastic parameters, c_{44}, N, A, used in this article by

$$S_{11}=S_{22}=(A/12c_{44})\frac{[(16N-11)+A(2N+1)]}{[-2(N+1)+A(2N+1)]+(2/A)},$$

$$S_{12}=(A/12c_{44})\frac{[(20N-7)-A(2N-1)]}{[-2(N+1)+A(2N-1)]-(2/A)},$$

$$S_{44}=S_{55}=(1/3c_{44})(2A+1),$$

$$S_{66}=(1/3c_{44})(A-2),$$

$$S_{15}=-S_{25}=-(1/2)S_{46}=(1/3\sqrt{2}c_{44})(1-A), \tag{10}$$

and the other parameters in the expressions for the stress components, Eq. (9), are defined as follows:

$$R^2=\frac{(16N-11)+A(2N-1)+(2/A)[-2(N+1)+A(2N-1)]}{(16N-11)+A(2N-1)-[2(A-4)/(2A+1)][-2(N+1)+A(2N-1)]},$$

$$\eta=(1/2c_{44})(A-1),\quad s_{11}=A/[2c_{44}(N+1)],\quad s_{12}=-AN/[2c_{44}(N+1)].$$

It can be seen from Eq. (9) that there are six stress components for a straight, pure $\langle 111\rangle$ screw dislocation by considering the anisotropy of elastic properties of the crystal. On setting $A=1$, then $S_{15}=0$, see Eq. (10), this yields $\sigma_1=\sigma_2=\sigma_3=\sigma_6=0$ from Eq. (9) and the expressions of σ_4 and σ_5 are reduced to that in isotropic materials.[39]

Substituting σ_m, Eq. (9), and Π_{mn}, the Appendix into Eq. (2) and then into Eq. (1), the expressions for ΔB_m and B_m are obtained. Finally, we obtain the intensity distribution in the birefringence image of a screw dislocation with Burgers vector b, $\langle 111\rangle$, viewed end-on in an elastically and photo-elastically anisotropic cubic crystal by substituting the expression of B_m into Eq. (8), which can be written as

$$\begin{aligned}I=(a^2b^2n_0^6\Delta l^2/144\lambda^2)[\{&\sqrt{6}(\pi_{12}-\pi_{13})x[(x^2-y^2)(x^2-3y^2)+2R^2y^2(3x^2-y^2)]+2\sqrt{2}[\pi_{11}-(1/2)(\pi_{12}+\pi_{13})\\&-\pi_{44}]y[2x^2(x^2-3y^2)-R^2(x^2-y^2)(3x^2-y^2)]-(S_{15}/S_{11})[\pi_{11}-(1/2)(\pi_{12}+\pi_{13})+2\pi_{44}]R^2y(x^2-y^2)\\&\times(3x^2-y^2)+\sqrt{3}(S_{15}/S_{11})(\pi_{12}-\pi_{13})R^2xy^2(3x^2-y^2)\}^2+4\{(-\sqrt{6}/2)(\pi_{12}-\pi_{13})y[2x^2(x^2-3y^2)\\&-R^2(x^2-y^2)(3x^2-y^2)]+\sqrt{2}[\pi_{11}-(1/2)(\pi_{12}+\pi_{13})-\pi_{44}]x[(x^2-y^2)(x^2-3y^2)+2R^2(3x^2-y^2)y^2]\\&+(S_{15}/S_{11})[\pi_{11}-(1/2)(\pi_{12}+\pi_{13})+2\pi_{44}]R^2xy^2(3x^2-y^2)+(\sqrt{3}/2)(S_{15}/S_{11})(\pi_{12}-\pi_{13})R^2y(3x^2-y^2)\\&\times(x^2-y^2)\}^2](R^2/Q^2S_{44}^2)\sin(2\alpha+2\beta),\end{aligned} \tag{11a}$$

TABLE I. The physical contents of YAG, YGG, Ge, and RbCl crystals.

Crystal	Lattice parameter	n_0	c_{44} (GPa)	c_{11} (GPa)	c_{12} (GPa)	Π_{11} $(\text{TPa})^{-1}$	Π_{12} $(\text{TPa})^{-1}$	Π_{44} $(\text{TPa})^{-1}$
YAG	12.005	1.832 $\lambda = 0.8\ \mu\text{m}$	115	324	112	0.120	0.050	−0.535
YGG	12.280	1.930 $\lambda = 0.6\ \mu\text{m}$	95.5	290.3	117.3	0.359	−0.057	0.827
Ge	5.6576	4.00 $\lambda = 10.6\ \mu\text{m}$	67.1	129	48	1.373	0.941	1.857
RbCl	3.749	1.48 $\lambda = 4\ \mu\text{m}$	4.70	36.4	6.3	7.04	2.99	−7.86

$$\tan 2\alpha = \{ -\sqrt{6}(\pi_{12}-\pi_{13})y[2x^2(x^2-3y^2) - R^2(x^2-y^2)(3x^2-y^2)] + 2\sqrt{2}[\pi_{11} - (1/2)(\pi_{12}+\pi_{13}) - \pi_{44}]$$
$$\times x[(x^2-y^2)(x^2-3y^2) + 2R^2(3x^2-y^2)] + 2(S_{15}/S_{11})[\pi_{11} - (1/2)(\pi_{12}+\pi_{13}) + 2\pi_{44}]R^2xy^2(3x^2-y^2)$$
$$+ \sqrt{3}(S_{15}/S_{11})(\pi_{12}-\pi_{13})R^2y(3x^2-y^2)(x^2-y^2)\}/\{\sqrt{6}(\pi_{12}-\pi_{13})x[(x^2-y^2)(x^2-3y^2)$$
$$+ 2R^2y^2(3x^2-y^2)] + 2\sqrt{2}[\pi_{11} - (1/2)(\pi_{12}+\pi_{13}) - \pi_{44}]y[2x^2(x^2-3y^2) - R^2(x^2-y^2)(3x^2-y^2)]$$
$$- (S_{15}/S_{11})[\pi_{11} - (1/2)(\pi_{12}+\pi_{13}) + 2\pi_{44}]R^2y(x^2-y^2)(3x^2-y^2)$$
$$+ \sqrt{3}(S_{15}/S_{11})(\pi_{12}-\pi_{13})R^2xy^2(3x^2-y^2)\}. \tag{11b}$$

IV. THE EFFECT OF ANISOTROPY ON BIREFRINGENCE IMAGE OF A ⟨111⟩ SCREW DISLOCATION VIEWED END-ON IN CUBIC CRYSTALS

As mentioned above, three independent elastic coefficients are required for elastically anisotropic cubic crystals, and the Zener ratio, $A = 2c_{44}/(c_{11}-c_{12})$, more truly represents the elastically anisotropy. For an elastically isotropic material, we have $A = 1$ and then $S_{15} = 0$, see Eq. (10).

In order to consider the anisotropy of photoelasticity in cubic crystal, the cubic classes divide into two groups. Four independent coefficients π_{11}, π_{12}, π_{13}, and π_{44}, are needed to define the photoelastic properties in classes 23 and $m3$, where the cube axes are diads; the other group, that is, classes $\bar{4}3m$, 432, and $m3m$, where the cube axes are tetrads, needs only three independent coefficients, π_{11}, π_{12}, and π_{44} with $\pi_{13} = \pi_{12}$. For the sake of characterization of the photoelastic anisotropy, two parameters are defined, that is, $D = \pi_{12}/\pi_{13}$ and $T = [\pi_{11} - (1/2)(\pi_{12} + \pi_{13})]/\pi_{44}$. For photoelastically isotropic materials, we have $D = 1$ and $T = 1$.

Equation (11) is the expression for the birefringence image of ⟨111⟩ screw dislocation viewed end-on for both elastically and photoelastically anisotropic cubic crystals, which belongs to 23 and $m3$ cube classes; and three anisotropic parameters A, T, and D, should be considered. On setting $D = 1$, that is, $\pi_{12} = \pi_{13}$, Eq. (11) is reduced to the expression for $\bar{4}3m$, 432, and $m3m$ cube classes. On setting $D = 1$ and $A = 1$, Eq. (11) is reduced to the expression for elastically isotropic but photoelastically anisotropic cubic crystals ($\bar{4}3m$, 432, $m3m$ classes) which was deduced by Ge *et al.* and used to explain the birefringence images of ⟨111⟩ screw dislocations viewed end-on observed in YAG and GGG crystals.[12] It is well known that the Zener ratio, A, of YAG and GGG is equal to 1.036 and 1.049, respectively, and thus YAG and GGG can be considered as approximately elastically isotropic crystals. On setting $D = 1$, $T = 1$, and $A = 1$ ($S_{15} = 0$), it can be seen from Eq. (11) that $I = 0$, that is, the screw dislocations viewed end-on in isotropic materials are invisible.

The aim of this section is to discuss the effect of anisotropy on the birefringence image. Therefore, we consider four kinds of cubic crystals with different typical anisotropic parameters as examples of structures. The ⟨111⟩ screw dislocation in some example structures such as RbCl and Ge may be not really exist.[39] However, this does not influence the discussion of the effect of anisotropy on the image. All four kinds of crystals considered belong to the $m3m$ class and thus $D = 1$. In order to determine the anisotropic parameters, the elastic compliances and the piezo-optical coefficients of all materials used in this paper are obtained from Landolt-Bornstein,[40] see Table I. The computer-simulated images of ⟨111⟩ screw dislocation viewed end-on in RbCl ($A = 0.312$; $T = 0.515$; $D = 1$), YAG($A = 1.036$; $T = 0.130$; $D = 1$), YGG($A = 1.104$; $T = 0.503$; $D = 1$), and Ge($A = 1.657$; $T = 0.866$; $D = 1$) crystals are obtained respectively according Eq. (11). As shown in Fig. 2(a). the contour of equal intensity in computer-simulated image of ⟨111⟩ screw dislocation in YAG crystal ($A = 1.036$) approximately, but not exactly, consists of two circles in contact with each other at the origin [the contour of equal intensity of image in an elastically isotropic ($A = 1$) but photoelastically anisotropic material exactly consists of two circles which was deduced by Ge and co-workers[12]]. The computer-simulated images of screw dislocations in RbCl and YGG are shown in Figs. 2(b) and 2(c). It is clear that the shapes of equal intensity

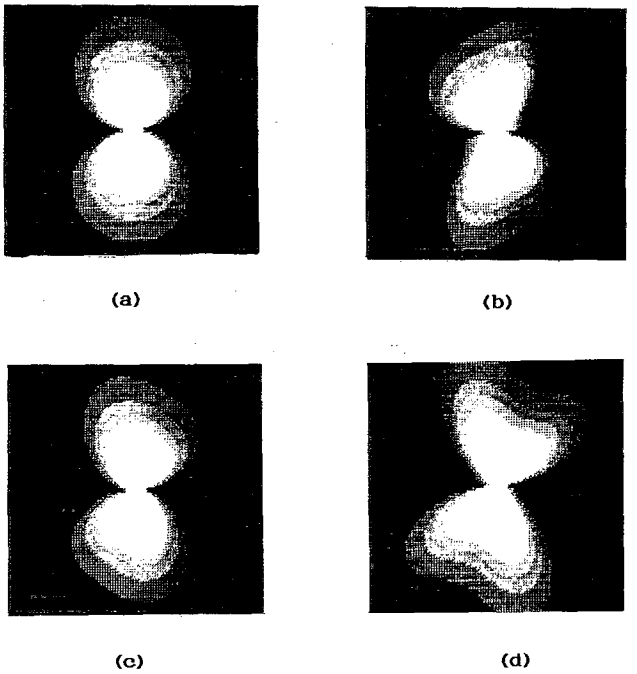

FIG. 2. The computer simulated images and effect of anisotropic parameters A and T on the birefringence images of a straight, pure screw dislocation with Burgers vector $a[111]$ viewed end-on in (a) YAG crystal with $A=1.036$, $T=0.130$, (b) RbCl crystal with $A=0.312$, $T=0.515$, (c) YGG crystal with $A=1.104$, $T=0.503$, (d) Ge crystal with $A=1.657$, $T=0.866$. The polarizer is parallel to $[11\bar{2}]$ of the wafer which is horizontal in each case, that is, $\beta=0°$.

contours deviate from the circles which mainly results from the deviation of Zener ratio A from unity; the photoelastic anisotropy of RbCl and YGG is smaller than that of YAG or the anisotropic parameter T of the two materials is closer to unity than that of YAG. The computer-simulated image of screw dislocation in a Ge crystal which has the largest Zener ratio A among these four kinds of crystals is shown in Fig. 2(d). By comparing Figs. 2(a), 2(c), and 2(d), it appears that the more the Zener ratio deviates from unity, the more the shape of equal intensity contour changes from circular. It may also be of interest to compare the relative intensities of birefringence images of [111] screw dislocations in the four kinds of crystals. From Eq. (11), it is clear that there are two factors which influence the relative intensity of birefringence image if the thickness of the crystal wafer, $\Delta 1$, and the amplitude of incident light, a, is given. One is $(b^2 n_0^6/\lambda^2)$ which can be calculated according to Table I. Thus ratio of the factors for YAG, YGG, Ge, and RbCl is $1.00{:}2.12{:}3.26\times10^{-2}{:}6.78\times10^{-3}$. The other is in heavy square brackets of Eq. (11) which results from the elastic stiffness constant: c_{11}, c_{12},c_{44}, and piezo-optical coefficient: Π_{11}, Π_{12}, Π_{44}, and can be obtained according to the relative grey levels in the computer simulation. The ratio of the factors for YAG, YGG, Ge, and RbCl is 1.00:1.12:31.6:1.70. It seems that the influence on the ratio of second factors results from Zener ratio mainly. On combining the two sets of factors, the ratio of relative intensities in birefringence images for YAG, YGG, Ge, and RbCl is $1.00{:}2.37{:}1.03{:}1.15\times10^{-2}$. Thus an assessment of birefringence topography for the characterization of dislocations for a given transparent crystal has been given.

It is to be noted that the cubic classes $\bar{4}3m$, 432, $m3m$, just discussed above, need to consider only two anisotropic parameters, A and T. However, three parameters, A, T, and D need to be considered in classes 23 and $m3$. We will discuss an example that belongs to $m3$ class, that is, $Ba(NO_3)_2$, in the next section.

V. COMPUTER-SIMULATED IMAGES AND EXPERIMENTAL IMAGES OF A ⟨111⟩ SCREW DISLOCATION IN $Ba(NO_3)_2$

The $Ba(NO_3)_2$ crystal belongs to the $m3$ class: three anisotropic parameters, A, T, D, are needed to define elastic and photoelastic anisotropicity. $Ba(NO_3)_2$ is a typical anisotropic crystal with large anisotropic parameters: $A=2.943$, $T=10.538$, $D=1.136$. It has been demonstrated by x-ray topography that the straight, pure screw dislocations with Burgers vector $a[111]$ really exist in $Ba(NO_3)_2$ crystals.[41] Therefore, we choose this crystal as an example in which the computer-simulated images and experimental images of ⟨111⟩ screw dislocation are obtained and compared with each other.

$Ba(NO_3)_2$ single crystal specimens were grown for aqueous solution. The feed materials (analytical reagent) of $Ba(NO_3)_2$ are commercially available and recrystallization from aqueous solution for three times was employed with refinement. The dominant impurities are Ca and Sr, present at less than 0.01%, respectively. The apparatus to grow crystals was in principle the same as that of Tsukamoto and Sunagawa[42] and Maiwa and co-workers.[41] The temperature fluctuation in the growth vessel were maintained <0.01 °C. A solution with saturation temperature at 34.00 °C was used. The ranges of the growth temperature and the supersaturation were 31.24 °C–33.51 °C and 1.01%–5.95%, respectively. The growth habit of the $Ba(NO_3)_2$ crystal is commonly constructed by {111} and {100} surfaces under the growth conditions, mentioned above. In the {111} growth sector, three types of dislocations were identified by x-ray topography,[41] that is, the edge dislocation, the screw dislocation, and the mixed dislocation with Burgers vector $a[1\bar{1}0]$, $a[111]$, and $a[110]$, respectively. Most of the dislocations are generated from the interface between seed crystals and regrown crystals or inherited from the seed. Once the growth conditions had stabilized, the dislocations ran almost normal to the (111) surface in the (111) growth sector and new dislocations were not generated. Thus, as the crystal grew the dislocation density decreased. More importantly, the tendency has led to large regions of crystal containing a few dislocations. The regions are suitable for direct observation of dislocations by means of birefringence topography. The crystal wafer, approximately 1.5–2.0 mm thick with surfaces parallel to (111) plane from the regions, mentioned above, was prepared by means of sawing the bulk crystal with rotating wet cotton thread, which gave no strain to a crystal by the operation. The wafer were then etched in water so as to eliminate the possible surface damage. Birefrin-

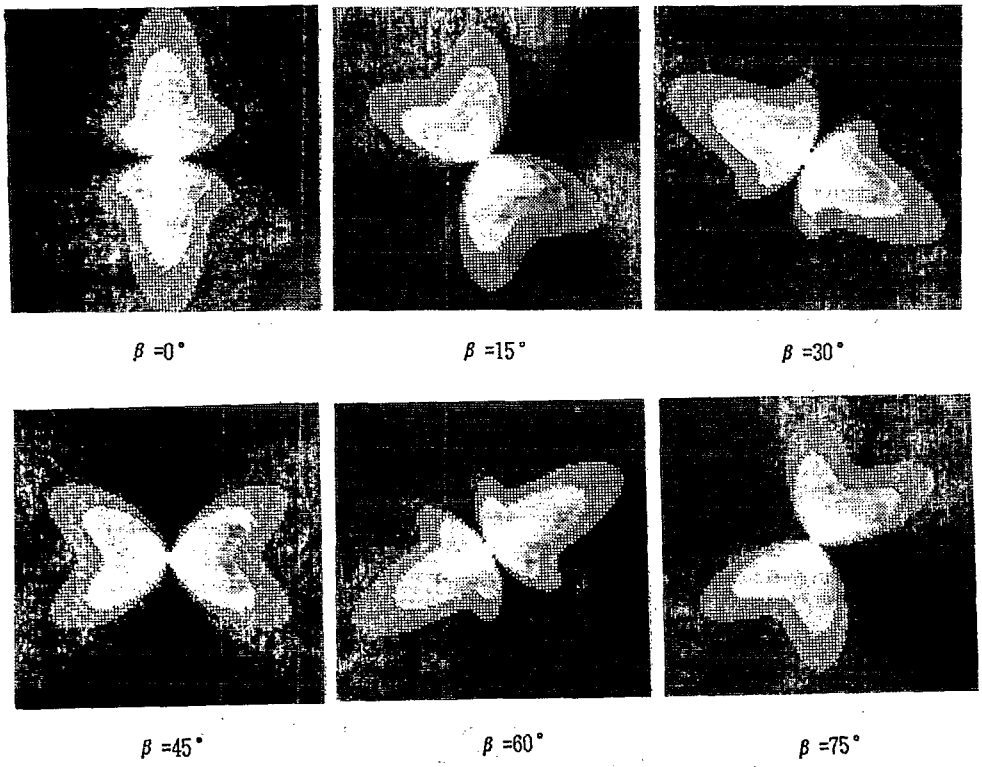

FIG. 3. Computer-simulated images of a straight, pure screw dislocation with Burgers vector $a[111]$ viewed end-on in $Ba(NO_3)_2$ crystal with $A=2.943$, $T=10.538$, $D=1.136$ for several orientations of the polarizer relative to $[11\bar{2}]$ direction of the wafer, that is, $\beta=0°$, 15°, 30°, 45°, 60°, 75°. The $[11\bar{2}]$ is horizontal in each case.

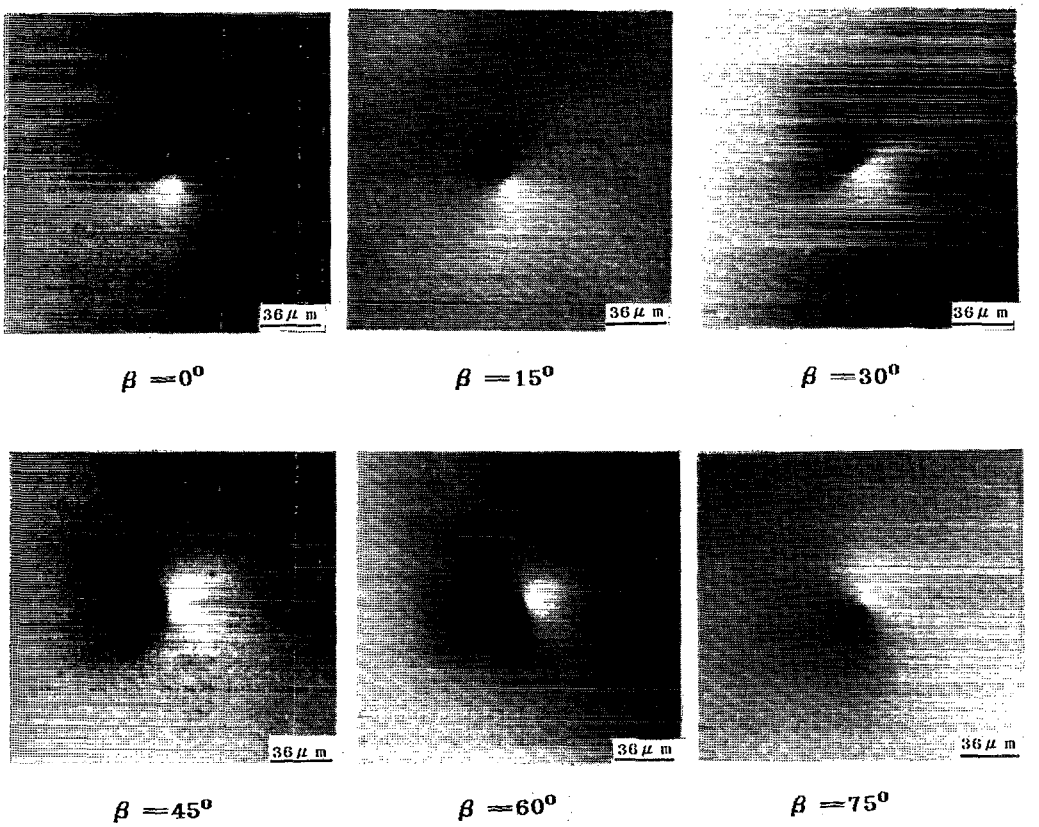

FIG. 4. Experimental images of a straight, pure screw dislocation with Burgers vector $a[111]$ viewed end-on in $Ba(NO_3)_2$ crystal for several orientations of the polarizer relative to the $[11\bar{2}]$ direction of the wafer, that is $\beta=0°$, 15°, 30°, 45°, 60°, 75°. The $[11\bar{2}]$ is horizontal in each case.

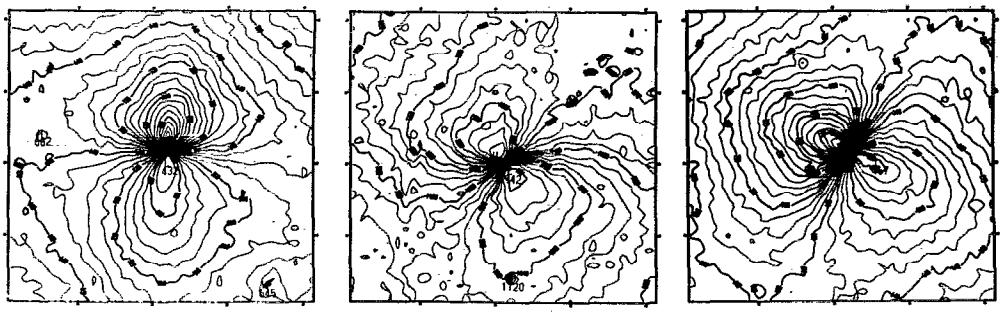

(a) $\beta = 0°$ (b) $\beta = 15°$ (c) $\beta = 30°$

FIG. 5. The contours of equal grey level of the negative films of the birefringence images of a pure screw dislocation viewed end-on in $Ba(NO_3)_2$ crystal shown in figs. 4 (a), 4(b), 4(c), measured by a microphotometer.

gence images of screw dislocations that had been determined by x-ray topography were observed in an Olympus vanox polarizing microscope. In order to eliminate the influence of the surface flatness on the birefringence images, the wafer observed was immersed in monomethylaniline, the refractive index, of which is very close to that of the $Ba(NO_3)_2$ crystal.

The computer-simulated images and experimental images of a straight, pure screw dislocation with Burgers vector $a[111]$ viewed end-on in the $Ba(NO_3)_2$ crystal are shown in Figs. 3 and 4, respectively, in which the images correspond to several orientations of the polarizer relative to the $[11\bar{2}]$ of the wafer, that is, $\beta = 0°$, 15°, 30°, 45°, 60°, 75°. The contours of equal grey level measured from the negative film of Fig. 4 by means of a microphotometer are shown in Fig. 5, in which the contours of the equal grey level only correspond to three orientations of the polarizer, that is $\beta = 0°$, 15°, 30°. On comparing Fig. 3–5, the shapes of contours of absolute value of equal intensity in the computer simulated images and experimental images are in good agreement. Obviously, the images observed in Fig. 4 show the black-white contrast in opposite petals which is still a problem to be solved in the future. However, it is a common phenomenon that the reversal of contrast in opposite petals of the experimental images of defects such as inclusions,[9,10] edge dislocations,[5,9,43–45] screw dislocations,[12] mixed dislocations,[25] subboundaries[43] is usually observed in real crystals in which internal strains due to thermal stresses, inhomogeneity of composition, lattice mismatch or other defects with a long-range strain field always exist. In order to explain this phenomenon, the intensity distribution in the images has been analyzed with a long-range plane strain superposed on the strainfield of inclusion in isotropic materials,[9] edge dislocations in isotropic materials[5,45,46] and in anisotropic materials,[12] and screw dislocations in elastically isotropic but photoelastically anisotropic materials.[13] Although this phenomenon in both elastically and photoelastically anisotropic materials has not yet been explained by the theory described above yet, we believe that it results from the same reason. It is worth noting that the images of a $\langle 111 \rangle$ screw dislocations viewed end-on in such a crystal shown in Fig. 3 $\beta = 0°$ and Fig. 4 $\beta = 0°$ are more complicated and widely different in the shape of the contours of equal intensity of the images from that in the class $m3m$ crystals shown in Fig. 2. It will be seen from this that the influence of large A, T, and also D, on the shape of equal intensity contours in image is of great importance.

APPENDIX

The transformation of elastic stiffness constant C_{mn} and piezo-optical coefficient Π_{mn} from the physical coordinate systems, [100], [010], [001], to the dislocation coordinate system $[11\bar{2}]$, $[\bar{1}10]$, [111].

For the purpose of transforming from the physical coordinate system to the dislocation coordinate system it is necessary to use the full four-index form of elastic stiffness and piezo-optical tensors. The tensors then obey the normal transformation rule:

$$A'_{ijkl} = l_{ip} l_{jq} l_{kr} l_{ls} \partial_{pqrs},$$

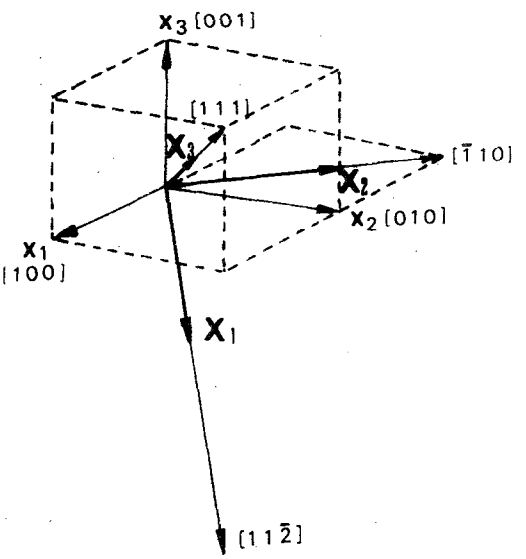

FIG. 6. Physical coordinate system [100], [010], [001] and dislocation coordinate system $[11\bar{2}]$, $[\bar{1}10]$, [111]. The x_1,x_2,x_3 and X_1,X_2,X_3 are unit vectors of coordinate axes of physical coordinates and dislocation coordinates, respectively, and $X_1 = (1/\sqrt{6})x_1 + (1/\sqrt{6})x_2 - (2/\sqrt{6})x_3$, $X_2 = -(1/\sqrt{2})x_1 + (1/\sqrt{2})x_2$, $X_3 = (1/\sqrt{3})x_1 + (1/\sqrt{3})x_2 + (1/\sqrt{3})x_3$.

where $l_{jq} = X_j \cdot x_q$ and X_j ($j=1,2,3$) are unit vectors along [11$\bar{2}$], [$\bar{1}$10], [111] axes, and x_q ($q=1,2,3$) are unit vectors along [100], [010], [001] (see Fig. 6).

In order to calculate the transformed component, we will use an abbreviated method, the direct inspection method, which is fully explained in Nye's book[35] (pp. 118–121, 133–135, 138, 139), so we will not go into details here, we just give the final results which are shown in following tensors:

The elastic stiffness constant in the coordinate system [11$\bar{2}$], [$\bar{1}$10], [111] for the cubic crystals [c_{mn}]:

$$
\begin{array}{cccccc}
\frac{1}{2}(C_{11}+C_{12}+2C_{44}) & \frac{1}{6}(C_{11}+5C_{12}-2C_{44}) & \frac{1}{3}(C_{11}+2C_{12}-2C_{44}) & 0 & -\frac{\sqrt{2}}{6}(C_{11}-C_{12}-2C_{44}) & 0 \\
\frac{1}{6}(C_{11}+5C_{12}-2C_{44}) & \frac{1}{2}(C_{11}+C_{12}+2C_{44}) & \frac{1}{3}(C_{11}+2C_{12}-2C_{44}) & 0 & \frac{\sqrt{2}}{6}(C_{11}-C_{12}-2C_{44}) & 0 \\
\frac{1}{3}(C_{11}+2C_{12}-2C_{44}) & \frac{1}{3}(C_{11}+2C_{12}-2C_{44}) & \frac{1}{3}(C_{11}+2C_{12}+4C_{44}) & 0 & 0 & 0 \\
0 & 0 & 0 & \frac{1}{3}(C_{11}-C_{12}+C_{44}) & 0 & \frac{\sqrt{2}}{6}(C_{11}-C_{12}-2C_{44}) \\
-\frac{\sqrt{2}}{6}(C_{11}-C_{12}-2C_{44}) & \frac{\sqrt{2}}{6}(C_{11}-C_{12}-2C_{44}) & 0 & 0 & \frac{1}{3}(C_{11}-C_{12}+C_{44}) & 0 \\
0 & 0 & 0 & \frac{\sqrt{2}}{6}(C_{11}-C_{12}-2C_{44}) & 0 & \frac{1}{6}(C_{11}-C_{12}+4C_{44})
\end{array}
$$

The piezo-optical coefficient in the coordinate system [11$\bar{2}$], [$\bar{1}$10], [111], for the cubic classes 23 and $m3$, [Π_{mn}]:

$$
\begin{array}{cccc}
\frac{1}{2}(\pi_{11}+\pi_{44})+\frac{1}{4}(\pi_{12}+\pi_{13}) & \frac{1}{6}(\pi_{11}-\pi_{44})+\frac{5}{12}(\pi_{12}+\pi_{13}) & \frac{1}{3}(\pi_{11}-\pi_{44})+\frac{1}{3}(\pi_{12}+\pi_{13}) & -\frac{\sqrt{6}}{6}(\pi_{12}-\pi_{13}) \\
\frac{1}{6}(\pi_{11}-\pi_{44})+\frac{5}{12}(\pi_{12}+\pi_{13}) & \frac{1}{2}(\pi_{11}+\pi_{44})+\frac{1}{4}(\pi_{12}+\pi_{13}) & \frac{1}{3}(\pi_{11}-\pi_{44})+\frac{1}{3}(\pi_{12}+\pi_{13}) & \frac{\sqrt{6}}{6}(\pi_{12}-\pi_{13}) \\
\frac{1}{3}(\pi_{11}-\pi_{44})+\frac{1}{3}(\pi_{12}+\pi_{13}) & \frac{1}{3}(\pi_{11}-\pi_{44})+\frac{1}{3}(\pi_{12}+\pi_{13}) & \frac{1}{3}(\pi_{11}+2\pi_{44}+\frac{1}{3}(\pi_{12}+\pi_{13}) & 0 \\
\frac{\sqrt{6}}{6}(\pi_{12}-\pi_{13}) & -\frac{\sqrt{6}}{6}(\pi_{12}-\pi_{13}) & 0 & \frac{1}{3}(2\pi_{11}+\pi_{44})-\frac{1}{3}(\pi_{12}+\pi_{13}) \\
-\frac{\sqrt{2}}{3}(\pi_{12}-\pi_{44})+\frac{\sqrt{2}}{6}(\pi_{12}+\pi_{13}) & \frac{\sqrt{2}}{3}(\pi_{11}-\pi_{44})-\frac{\sqrt{2}}{6}(\pi_{12}+\pi_{13}) & 0 & \frac{\sqrt{3}}{3}(\pi_{12}-\pi_{13}) \\
\frac{\sqrt{3}}{6}(\pi_{12}-\pi_{13}) & -\frac{\sqrt{3}}{6}(\pi_{12}-\pi_{13}) & 0 & \frac{\sqrt{2}}{3}(\pi_{11}-\pi_{44})-\frac{\sqrt{2}}{6}(\pi_{12}+\pi_{13})
\end{array}
$$

$$
\begin{array}{cc}
-\frac{\sqrt{2}}{3}(\pi_{11}-\pi_{44})+\frac{\sqrt{2}}{6}(\pi_{12}+\pi_{13}) & -\frac{\sqrt{3}}{6}(\pi_{12}-\pi_{13}) \\
\frac{\sqrt{2}}{3}(\pi_{11}-\pi_{44})-\frac{\sqrt{2}}{6}(\pi_{12}+\pi_{13}) & \frac{\sqrt{3}}{6}(\pi_{12}-\pi_{13}) \\
0 & 0 \\
-\frac{\sqrt{3}}{3}(\pi_{11}-\pi_{13}) & \frac{\sqrt{2}}{3}(\pi_{11}-\pi_{44})-\frac{\sqrt{2}}{6}(\pi_{12}+\pi_{13}) \\
\frac{1}{3}(2\pi_{11}+\pi_{44})-\frac{1}{3}(\pi_{12}+\pi_{13}) & \frac{\sqrt{6}}{6}(\pi_{12}-\pi_{13}) \\
-\frac{\sqrt{6}}{6}(\pi_{12}-\pi_{13}) & \frac{1}{3}(\pi_{11}+2\pi_{44})-\frac{1}{6}(\pi_{12}+\pi_{13})
\end{array}
$$

[1] W. C. Bond and J. Audrus, Phys. Rev. **101**, 1211 (1956).
[2] R. Bullough, Phys. Rev. **110**, 620 (1958).
[3] V. C. Indenbom, V. I. Nikitenko, and I. S. Mitevskii, Sov. Phys. Solid State **4**, 162 (1962).
[4] D. J. Fathers and B. K. Tanner, Philos. Mag. **28**, 749 (1978).
[5] B. K. Tanner and D. J. Fathers, Philos. Mag. **29**, 1081 (1974).
[6] J. W. Matthews and T. S. Plaskett, Phys. Status Solidi A **37**, 499 (1976).
[7] D. A. Jenkins, T. S. Plaskett, and P. Chaudhari, Philos. Mag. A **39**, 237 (1979).
[8] S.-S. Jiang, and A. R. Long, Philos. Mag. A **56**, 367 (1987).
[9] S.-Y. Shu, C.-Z. Ge, and D. Feng, J. Phys. (Paris) Colloq. **41**, C6-186 (1980).
[10] J. W. Mathews, E. Klokholm, V. Sadagopan, T. S. Plaskett, and E. Mendel, Acta Metall. **21**, 203 (1973).
[11] D. J. Fathers and B. K. Tanner, Philos. Mag. **27**, 17 (1973).
[12] C.-Z. Ge, N.-B. Ming, and D. Feng, Philos. Mag. A **53**, 285 (1986).
[13] C.-Z. Ge, J. Zhang, and D. Feng, Acta Phys. Sinica **36**, 1081 (1987); Chin. Phys. **8**, 638 (1988).
[14] B. Cockayne and J. M. Roslington, J. Mater.Sci. **8**, 601 (1973).
[15] W. Schmidt and R. W. Weiss, J. Cryst. Growth **43**, 55 (1978).
[16] M. J. Prescott and J. Basterfield, J. Mater. Sci. **2**, 583 (1967).
[17] J. W. Mathews and T. S. Plaskett, Philos. Mag. **33**, 73 (1976).
[18] J. W. Mathews, E. Klokholm, T. S. Plaskett, and V. Sadagopan, Phys. Status Solidi A **19**, 671 (1973).
[19] C. Becker, E. Zsoldos, and A. Weber, Phys. Status Solidi A **34**, 519 (1976).
[20] J. W. Mathews and T. S. Plaskett, J. Mater. Sci. **13**, 2029 (1978).
[21] W. T. Stacy, J. A. Pistorius, and M. M. Janssen, J. Cryst. Growth **22**, 37 (1974).
[22] C.-Z. Ge, X.-Y. Xu, and D. Feng, Acta Phys. Sinica **30**, 218 (1981).
[23] C.-Z. Ge, X.-Y. Xu, and D. Feng, Acta Phys. Sinica **31**, 415 (1982).
[24] N.-B. Ming and Y.-S. Yang, Acta Phys. Sinica **28**, 285 (1979).
[25] H. Booyans and J. H. Basson, J. Appl. Phys. **51**, 4368, 4375 (1980); **52**, 4112 (1981).
[26] J. S. Ahearn, C. A. B. Ball, and C. Laird, Phys. Status. Solidi A **38**, 315 (1976).
[27] J. Hilgarth, J. Mater. Sci. **13**, 2697 (1978).
[28] F. K. Reinhart and R. A. Logan, J. Appl. Phys. **44**, 3171 (1973).
[29] K. Loschke and P. Pauller, Philos. Mag. A **46**, 699 (1982).
[30] M. Zafar Iqbal, J. Mater. Sci. **15**, 781 (1980).
[31] G. B. Stringfellow, P. F. Lindquist, T. R. Cass, and R. A. Burmeister, J. Electron. Mater. **3**, 497 (1974).
[32] J. W. Mathews, T. S. Plaskett, and S. E. Blum, J. Cryst. Growth **42**, 621 (1977).
[33] S. F. Nygren, J. Cryst. Growth **19**, 21 (1973).
[34] W. J. P. Van Enckevort and W. H. Van der Linden, J. Cryst. Growth **47**, 196 (1979).
[35] J. F. Nye, *Physical Properties of Crystals* (Oxford, London, 1957), p. 41.
[36] M. Born and E. Wolf, *Principles of Optics* 6th ed. (Pergamon, London, 1980), p. 694.
[37] Y. T. Chou and T. E. Mitchell, J. Appl. Phys. **38**, 1535 (1967).
[38] A. N. Stroh, Philos. Mag. **3**, 625 (1958).
[39] J. P. Hirth and J. Lothe, *Theory of Dislocations*, 2nd ed. (McGraw-Hill, New York, 1982).
[40] K. H. Hellwege, *Elastic, Piezoelectric, Pyroelectric, Piezooptic, Electrooptic Constants and Nonlinear Dielectric Susceptibilities of Crystals*, Landolt-Bornstein, New Series (Springer, Berlin, 1979), Vol. 11.
[41] K. Maiwa, K. Tsukamoto, and I. Sunagawa, J. Cryst. Growth **82**, 611 (1987).
[42] K. Tsukamoto and I. Sunagawa, J. Cryst. Growth **63**, 18 (1983).
[43] X.-Y. Xu and D. Feng, J. Mater. Sci. **20**, 612 (1985).
[44] H. S. Bagdasarov and L. M. Doduk, Kristallogr. **15**, 334 (1970).
[45] V. L. Indenbohm, Dokl. Akad. Nauk S.S.S.R. **141**, 1360 (1961).
[46] D. A. Jenkin and J. J. Hren, Philos. Mag. **33**, 173 (1976).